Desalination and Water Treatment
www.deswater.com

doi: 10.1080/19443994.2013.782830

52 (2014) 283–292
January

Taylor & Francis
Taylor & Francis Group

Adsorption of Sn(II) on expanded graphite: kinetic and equilibrium isotherm studies

Ming Yang[a,b], Yinghua Zhao[b], Xiuzhi Sun[b], Xiantao Shao[b], Dengxin Li[b,*]

[a]*Research Center of Analysis & Measurement, Donghua University, 2999 North Renmin Road, Shanghai 201620, China*
[b]*School of Environmental Science and Engineering, Donghua University, 2999 North Renmin Road, Shanghai 201620, China*
Tel. +86 21 67792541; Fax: +86 21 67792522; email: lidengxin@dhu.edu.cn

Received 13 December 2012; Accepted 3 March 2013

ABSTRACT

Expanded graphite (EG) was prepared by microwave irradiation at 1000 W for 60 s. EG is a novel adsorbent for Sn(II) adsorption and its ability to remove Sn(II) ions from wastewater was investigated. To characterize the adsorptive characteristics of the produced EG, the microstructures of the resultant EG were observed using scanning electron microscopy. Chemical characterization of the surface resultant EG was studied by Fourier transform infrared spectroscopy. The effects of pH, adsorbent dosage, initial concentration, temperature, and contact time on the adsorption surface were studied using the batch process technique. The data fitted with the Langmuir equilibrium isotherm and pseudo-second-order kinetics. The maximum adsorption capacity of Sn(II) on the resultant EG was 378.78 mg g^{-1}.

Keywords: Adsorption; Expanded graphite; Stannum adsorption; Isotherm

1. Introduction

In recent years, a variety of heavy metals have been discharged into natural waters. These come from processes such as metal plating, acid battery manufacturing, glass operation, and electroplating [1]. Stannum is a by-product of the electroplating industry and is harmful to human health. In the process of preparing Sn(II), inhaling tin dust may cause chronic bronchitis, and contact with stannous chloride will cause eczema. It is therefore important to reduce the concentration of Sn(II) in aqueous solutions using various methods. Nowadays, the most widely used methods for removing harmful metals from wastewater include ion exchange, ferrite precipitation, reverse osmosis, membrane filtration, and adsorption [2].

The method of adsorption has been shown to be an effective method for removing harmful metals. Zhang et al. used solid products as adsorbents to adsorb Sn (II), with removal rates of up to 91.8% [3]. Cheng Shixian used activated carbon as an adsorbent to remove Sn(II) with the adsorption quantity reaching 1 g g^{-1} [4]. Activated carbon is one of the most effective adsorbents for removing heavy metals. Despite its widespread use in industry, activated carbon remains an expensive material. Therefore, it is necessary to produce low cost and effective adsorption materials that can be applied to water pollution control.

*Corresponding author.

Expanded graphite (EG) is a poriferous material and has a wide range of pore diameters and a large pore volume. EG is a good adsorbent due to the network pore structure, weak polarity, hydrophobic and lipophilic nature with extremely high selective sorption capacity to large organic compounds with weak polarity from water [5]. EG becomes increasingly important because of numerous actual and potential applications in fuel cells [6], hydrogen storage [7], catalysts [8], sensors [9], biomedical materials [10] and adsorbents. In the present study, the results of adsorption experiments of EG onto tin ions at various pH values, temperatures, adsorbent dosages, initial concentrations, and adsorption times are discussed. The aim of this study is to characterize the main factors controlling the adsorption mechanism of EG to stannum ions and to describe the adsorption models. The treatment of Sn in wastewater is also studied.

2. Materials and methods

2.1. Preparation and analysis of stannum solution

A 1,000 mg L^{-1} stock solution of stannum was prepared by dissolving an appropriate amount of $SnCl_2$ in 1 mol L^{-1} HCl. Working solutions were prepared by further dilution from the stock solution. All reagents were of analytical grade. Ion concentration was measured by ICP-OES (Prodigy, America). The pH values were measured by a pH meter (METTLER TOLEDO FE20).

2.2. Preparation of EG

Commercial expandable graphite (expansion ratio of 150–250 mL g^{-1}, purchased from Qingdao Nanshu Hongda Graphite Co. Ltd., China) was directly placed into a Sanyo MW oven (EM-3011EB1) and irradiated at 1,000 W for 60 s.

2.3. Adsorbents characterization

The surface morphology of the EG was characterized with scanning electron microscopy (SEM) (JSM-5600LV, JEOL Ltd., Japan). The porous characteristics of the EG were determined by the adsorption of N_2 using specific surface area pore size analyzer (BK122T-B, JWGB Ltd., China). The composition of the EG and the material which was adsorbed by EG were analyzed by energy dispersive spectrometer (EDS, IE 300×). Chemical characteristics were studied by Fourier transform infrared spectroscopy (FTIR) in order to identify the functional groups at the surface of EG. FTIR spectra were recorded with a TENSOR27 IR (Bruker Co., Germany) spectrometer.

2.4. Adsorption experiments

The effects of experimental parameters on the stannum ion adsorption were studied in batch operation mode. The stock solution of Sn(II) was prepared by dissolving $SnCl_2$ in 1 mol L^{-1} HCl. Working solutions were obtained by further dilutions from the stock solution. The pH of the working solutions was adjusted by adding 0.1 mol L^{-1} HCl or NaOH solutions. Adsorption experiments were performed by shaking (0.005–0.02 g) of adsorbent with 25 mL of a working experimental solution of known concentration in a temperature-controlled water bath shaker. Finally, the supernatant liquids were filtered and the metal concentration in each vial was determined using ICP-OES. The temperature-controlled water bath shaker (SHZ-88) was used to control the desired temperature. The recorded data was used to calculate the adsorption capacity (q) using the following equation:

$$q = \frac{[(C_0 - C_e)V]}{m} \quad (1)$$

where q is the amount of metal ions adsorbed onto a unit amount of adsorbent (mg g^{-1}); C_0 and C_e are the initial and equilibrium solution concentrations (mg L^{-1}), respectively; V is the volume of aqueous phase (L); and m is the mass of the adsorbent (g).

3. Results and discussion

3.1. Resulting structures

The microstructure of the EG is shown in Fig. 1 (a)–(d). Fig. 1(a) shows the structure of the adsorbent. From Fig. 1(b), it can be seen that the porous (Fig. 1(c)) structure was made up of many parallel and collapsed layers. It can be seen in Fig. 1(c) that the furrow resulting from the parting of packed layers can provide channels to facilitate the transport of working fluids. Therefore, the EG might have a high removal rate [11]. The collapsed layers made up of nanoscale graphite pieces are shown in Fig. 1(d).

The performance of the adsorbent is improved by more adsorptive sites of larger surface area and more of internal pore structure. Pore size distributions (PSDs) of the EG are presented in Fig. 2(a)–(d). Fig. 2(a) and (b) shows the N_2 adsorption/desorption integral distribution curve of the EG. Fig. 2(c) and (d) shows the N_2 adsorption/desorption differential curve of the adsorbent. The Brunauer–Emmett–Teller (BET) surface area was calculated using the BET equation from the selected N_2 adsorption data; micropore size distribution was obtained by the Barrett–Joyner–Halenda

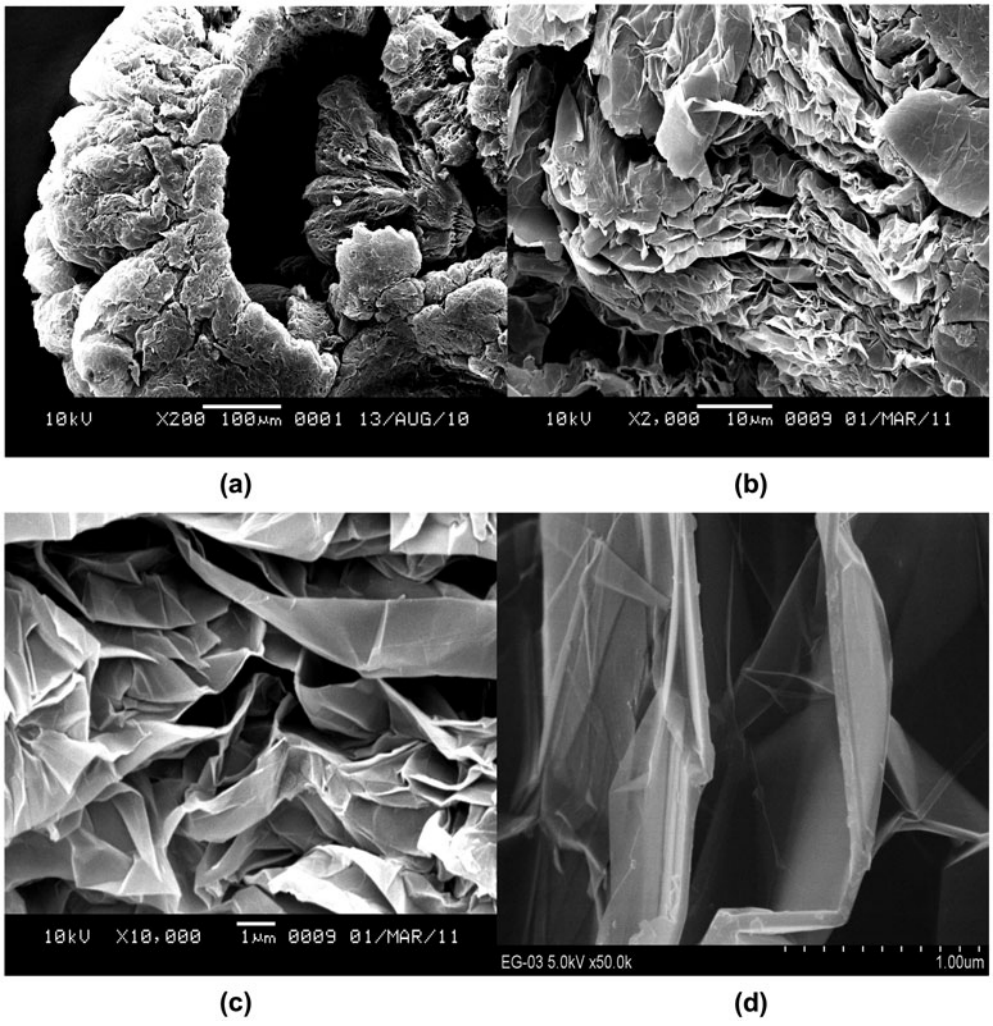

Fig. 1. SEM of EG.

method. It can be concluded that the BET specific surface area (S_{BET}) was 61.17 $m^2 g^{-1}$, micropore volume (V_m) was 14.03 $cm^3 g^{-1}$, and the most probable pore size was 3.91 nm.

The composition of EG and the material which was adsorbed by EG are shown in Fig. 3. The EDS spectrum image is presented in Fig. 3, where the presence of C, O, and Sn confirms that Sn(II) is adsorbed into the pores.

Fig. 4 shows the IR spectra of EG. The bands around 3,448 cm^{-1} are present in the spectra and represent the stretching and bending vibrations of the –OH functional group of H_2O [12]. The peaks at 2,920 and 2,852 cm^{-1} represent the symmetrical stretching vibration of its $–CH_2$ group [13]. The bands around 1,064 cm^{-1} are the characteristic bands of the stretching vibration mode of C–O–C.

3.2. Adsorption rate

3.2.1. Effect of pH

The pH value is an important parameter controlling adsorption processes because of its influence on the sorbents and sorbate parameters [14,15]. The adsorption behavior of Sn on the EG was therefore investigated at different pH ranging from 1 to 4 at room temperature. With an initial stannum ion concentration of 200 mg L^{-1}, adding 0.01 g of EG separately into the four groups of stannum ion solutions resulted in the four final pH values being 1.55, 2.10, 2.51, and 3.12. As stannum precipitates at higher pH values, pH values beyond 4 were not tested.

Fig. 5 shows the effect of different pH values on the removal of Sn(II) by EG. With increased pH, the removal rate and adsorption quantity also increased.

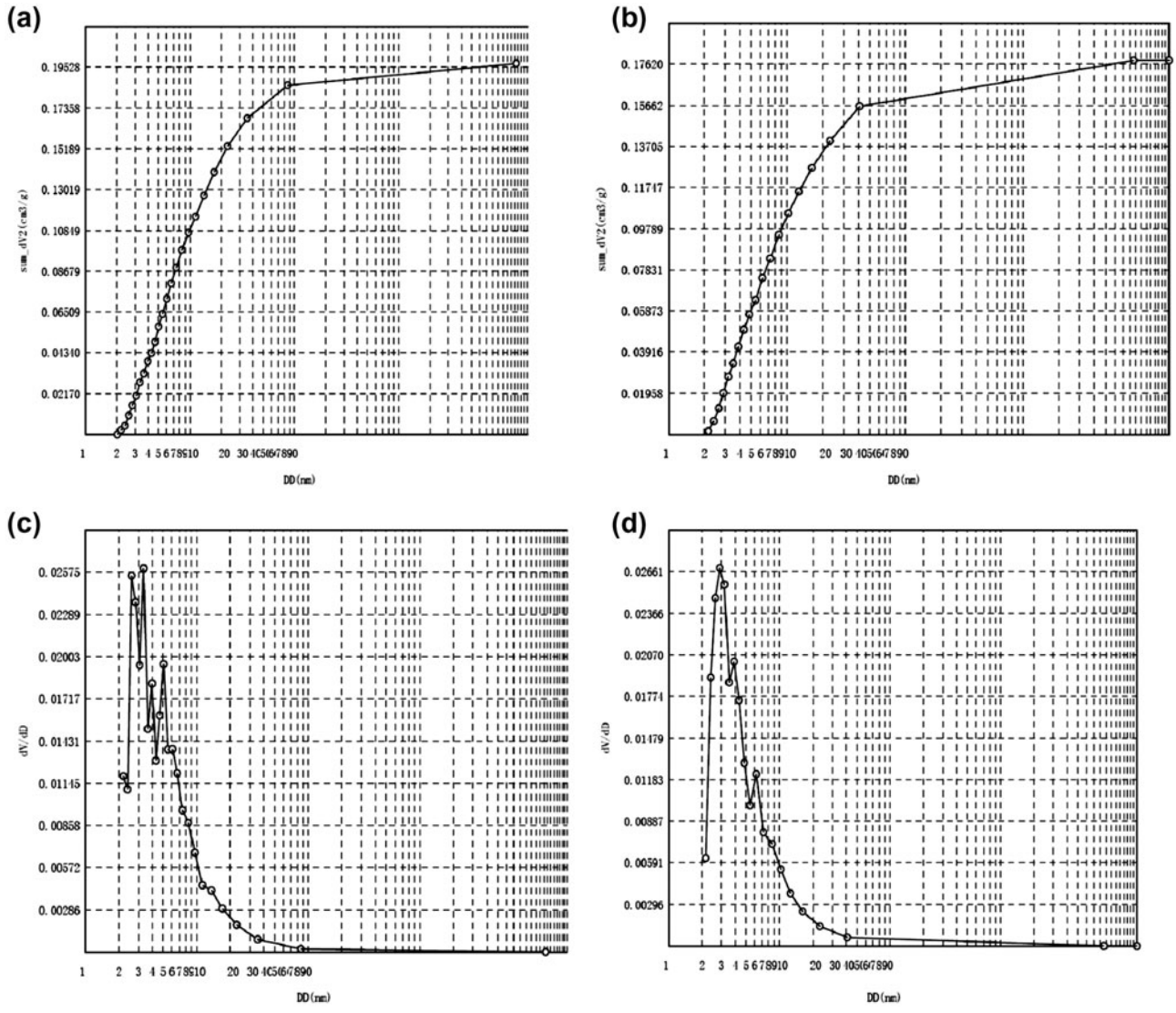

Fig. 2. Adsorption/desorption pore size distribution curves of EG.

When pH was 2.51, the removal rate of Sn(II) reached 80%. These results show that pH is a very important factor in the adsorption of Sn(II). The results can be explained based on the competition between Sn(II) and H_3O^+ for adsorption sites on EG. At low pH levels, excess H_3O^+ could compete with Sn(II) resulting in a low level of adsorbed Sn(II). When the pH level increases, the covered H_3O^+ leaves the porous layer activated charcoal surface and makes the sites available to Sn(II).

3.2.2. Effect of adsorbent dosage

The effect of adsorbent dosage was tested with an initial Sn(II) concentration of 200 mg L^{-1}, adding 0.005, 0.01, 0.015, and 0.02 g of EG separately in four groups at pH 2.1 at 25 °C. The results are shown in Fig. 6.

Fig. 6 shows the evolution of the removal rate of Sn(II) with increasing adsorbent dosage. The removal rate increased with the dosage, with the removal rate reaching 80% when the dosage increased to 0.015 g.

With the increase of EG amounts, the surface area of EG increases, which means that there were more ''active points'' available to absorb Sn(II). This resulted in increasing amount of Sn(II) on the absorbent. Therefore, while the solution with certain concentrations of Sn(II) reaches an adsorption equilibrium, the residue Sn(II) concentration in wastewater decreases continuously as the removal rate increases. However, the removal rate tends to stabilize when a certain amount of EG is added. This indicates that the

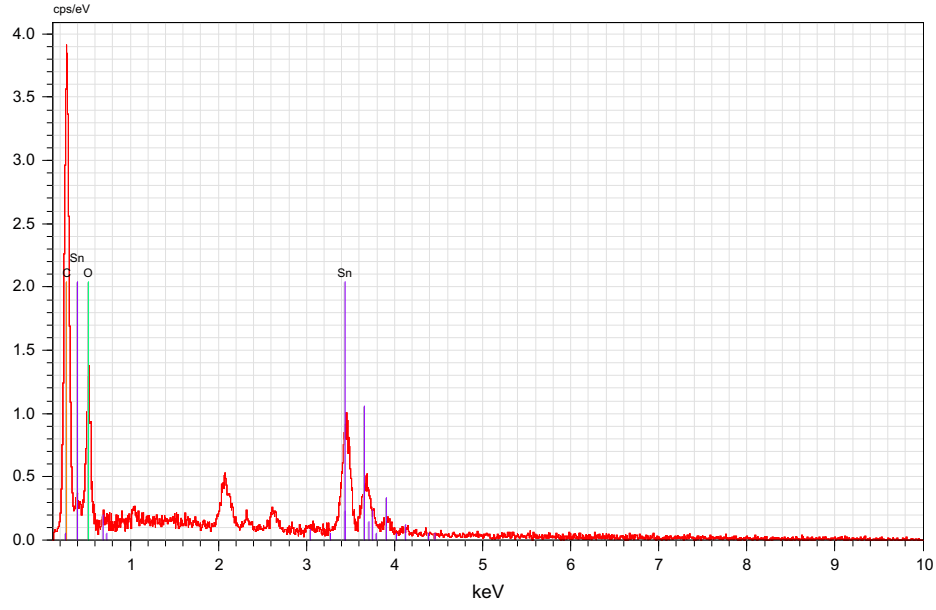

Fig. 3. EDS of after adsorption of EG.

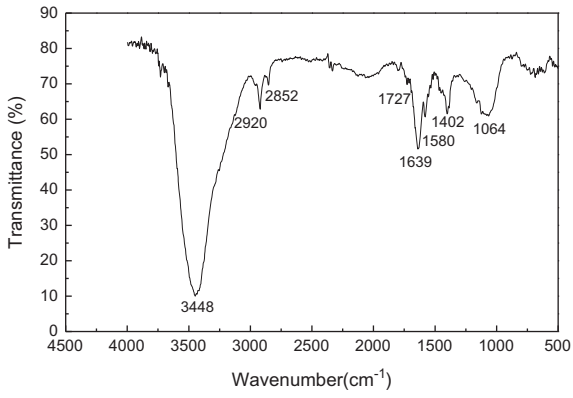

Fig. 4. FTIR of EG.

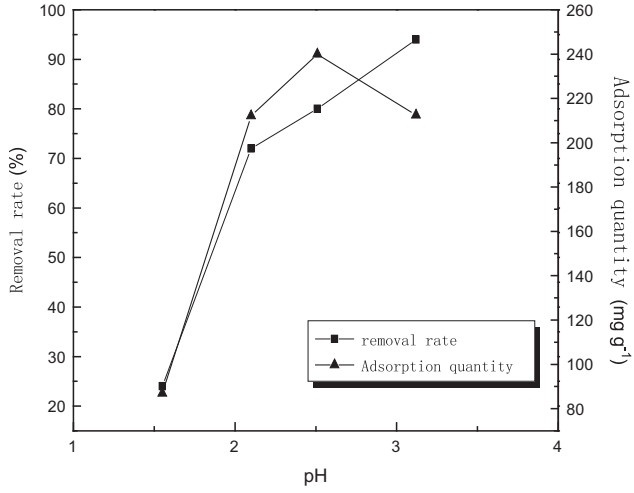

Fig. 5. Effect of the initial pH on adsorption of Sn(II) by EG.

absorption of Sn(II) by EG has reached a saturation point, and addition of EG beyond this point has no effect on Sn(II) removal.

3.2.3. *Effect of initial concentration*

The initial Sn(II) concentrations were 100–300 mg L^{-1}. About 0.02 g of EG was added separately into those five groups of stannum ion solution before adjusting the pH to 2.5 at 25 °C. The results are shown in Fig. 7.

It can be seen in Fig. 7 the removal rate decreased with increasing initial concentration, but the adsorption quantity increased with increasing concentration. When the initial concentration reached 300 mg L^{-1}, the adsorption was 343.42 mg g^{-1}. This is because Sn(II) at low concentrations can fully occupy the EG active points, while with higher Sn(II) concentrations, there are not enough active points to accommodate more Sn (II). The restriction of EG aperture and electrostatic repulsion between Sn(II) can also cause the removal rate of Sn(II) to decrease. The diffusion rate of Sn(II) of EG increased with concentration and the Sn(II) adsorbed on specific surface area of EG increased which increases the adsorbed amount and tends to balance the EG usage at a certain amount.

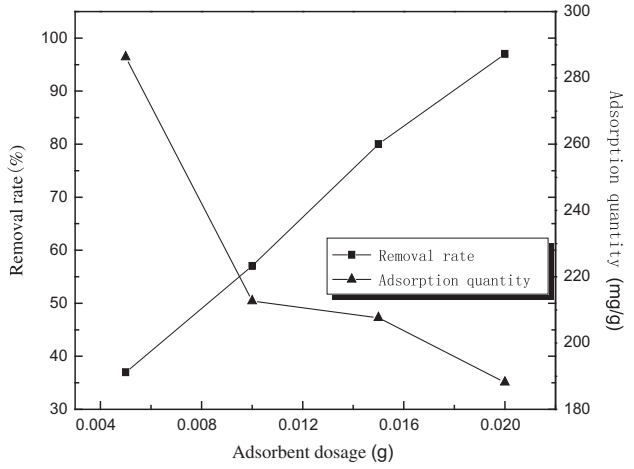

Fig. 6. Effect of adsorbent dosage on adsorption of Sn(II) by EG.

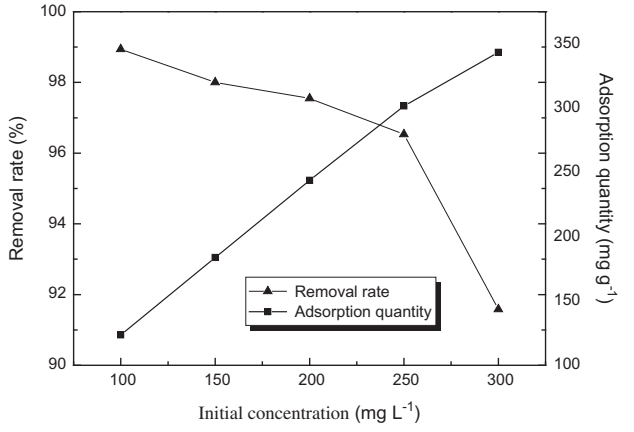

Fig. 7. Effect of initial concentration on adsorption of Sn(II) by EG.

3.2.4. Effect of temperature

About 0.01 g of EG was added into a group of stannum ion solution of 200 mg L^{-1} at pH 2.5 separately at different temperatures ranging from 20 to 50°C.

Fig. 8 shows the removal rate and adsorption quantity at different temperatures. The adsorption capacity of EG increased with increased temperature. The best adsorption capacity of EG was at 50°C, with the removal rate reaching 94%.

3.2.5. Effect of time

The initial Sn(II) concentration was 200 mg L^{-1}, 0.02 g of EG was added into the groups of stannum ion solution. The pH was adjusted to 2.5, the temperature was 25 °C, and the adsorption time was from 5 to 120 min.

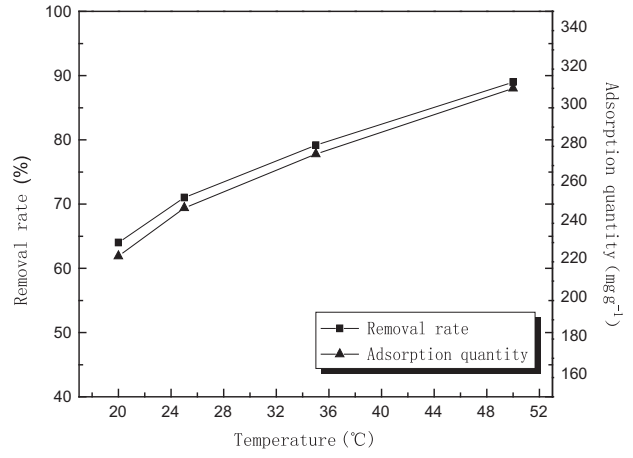

Fig. 8. Effects of temperature on the adsorption of Sn(II) by EG.

Fig. 9 shows the change in removal rate and adsorption quantity as the time increased from 5 to 120 min. When the time reached 60 min, the adsorption was almost balanced, and the removal rate reached 97% while the adsorption quantity was 243.88 mg g^{-1}.

The reason for high absorption rates at the beginning was Sn(II) being adsorbed on the outer surface of EG. The procedure for adsorption involves the absorbent changing from macroporous to microporous though transition pores. The Sn(II) transition rate decreases when the pore size becomes small. Removal rate and adsorption amounts increase slowly with time until equilibrium is reached. Meanwhile, the equilibrium time of Sn(II) absorption depends on initial concentration. Considering all factors, 120 min was selected as a suitable absorption time for dynamic equilibrium.

EG has proved to be an effective and novel adsorbent for the removal of Sn(II) from aqueous solution.

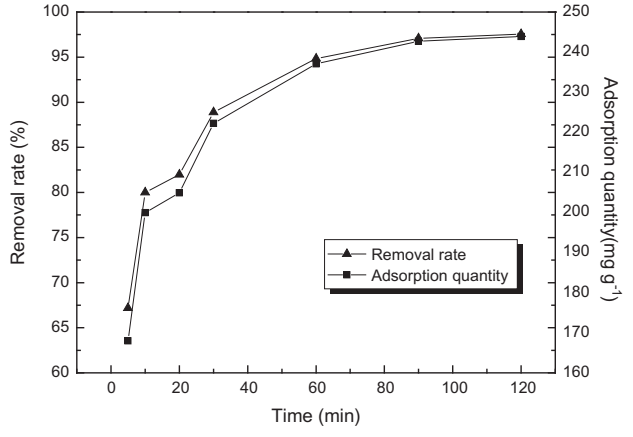

Fig. 9. Effects of contact time on the adsorption of Sn(II) by EG.

The adsorption is highly dependent on pH, adsorbent dosage, initial concentration, and temperature. The highest removal efficiency of Sn(II) is about 98%.

3.3. Adsorption isotherms

3.3.1. Langmuir isotherm

The Langmuir method assumes that the adsorption occurs uniformly on the active part of the surface, and other molecules do not interact with this active part when a molecule is adsorbed on an active site.

The Langmuir equation can be written as:

$$q_e = \frac{Q^0 b C_e}{1 + bC_e} \text{(Non-linear form)} \quad (2)$$

$$\frac{C_e}{q_e} = \frac{1}{Q^0 b} + \frac{C_e}{Q^0} \text{ (Linear form)} \quad (3)$$

where q_e is the amount of solute adsorbed per unit weight of adsorbent (mg g^{-1}), C_e is the equilibrium concentration of solute in the bulk solution (mg L^{-1}), Q^0 is the monolayer adsorption capacity (mg g^{-1}), and b is the constant which is related to the free energy of adsorption. The constants of the Langmuir isotherm are obtained by plotting $\frac{C_e}{q_e}$ vs. C_e (Fig. 10).

3.3.2. Freundlich isotherm

The Freundlich isotherm may be written as:

$$q_e = K_f C_e^{1/n} \text{ (Non-linear form)} \quad (4)$$

$$\ln q_e = \ln K_f + \frac{1}{n} \ln C_e \text{ (Linear form)} \quad (5)$$

where K_f is the constant indicative of the relative adsorption capacity of the adsorbent (mg g^{-1}) and $1/n$ is the constant indicative of the intensity of the adsorption. The constants of the Freundlich isotherm are obtained by plotting $\log q_e$ vs. $\log C_e$ (Fig. 11).

Langmuir and Freundlich constants are given in Table 1. The higher correlation coefficient for EG ($R^2 = 0.9982$) shows that the Langmuir model is more suitable than the Freundlich model for the adsorption equilibrium of Sn(II). Therefore, the adsorption of Sn(II) by EG is considered to be monomolecular adsorption.

3.4. Kinetics of adsorption

The study of adsorption kinetics is significant and can provide valuable insights into the reaction pathways. Some types of kinetic models are used to explain the mechanism of the adsorption reaction. The most common models are pseudo-first-order equation and pseudo-second-order equation. The pseudo-first-order model is given by the Lagergren equation:

$$\log(q_e - q) = \log q_e - \frac{k_1 t}{2.303} \quad (6)$$

where q_e and q are the amounts of Sn(II) adsorbed (mg g^{-1}) at equilibrium time and any time, t, respectively, and k_1 is the rate constant of adsorption (min^{-1}). Plot of $\log(q_e - q)$ vs. t gives a straight line for pseudo-first-order adsorption kinetics which allows computation of the rate constant k_1 (Fig. 12).

On the other hand, the second-order equation based on equilibrium adsorption [16] is expressed as:

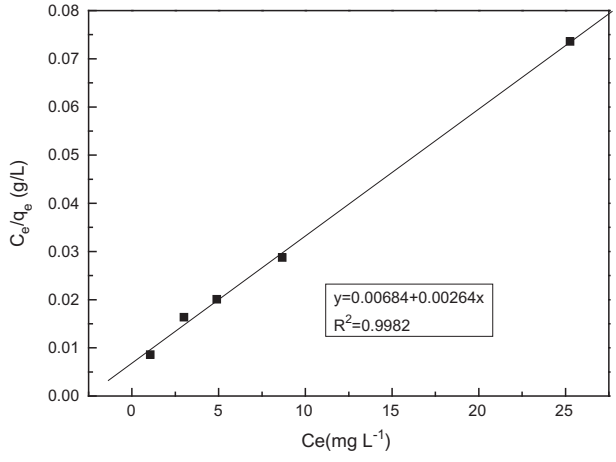

Fig. 10. The Langmuir adsorption isotherms for Sn(II) adsorption by EG.

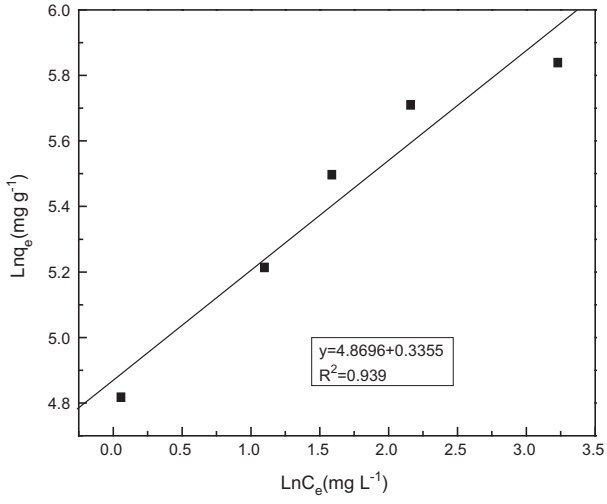

Fig. 11. The Freundlich adsorption isotherms for Sn(II) adsorption by EG.

Table 1
Langmuir and Freundlich isotherm constants for stannum adsorption on the EG

Adsorbent	Langmuir			Freundlich		
EG	Q^0	b	R^2	K_f	$1/n$	R^2
	378.78	0.386	0.9982	130.2688	0.3355	0.939

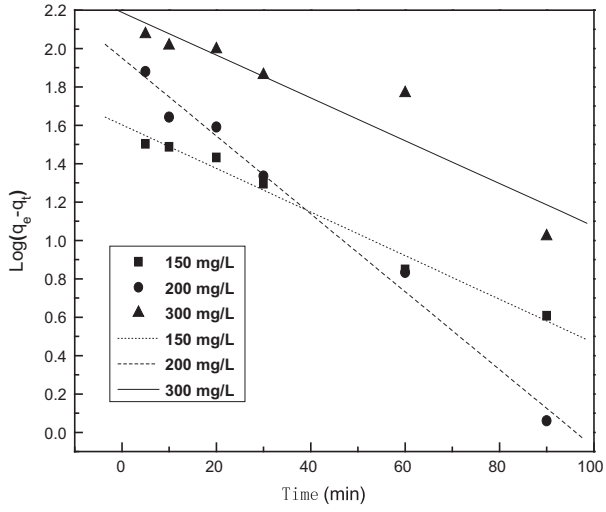

Fig. 12. Pseudo-first order kinetic plots for the removal of Sn(II) by EG at room temperature.

$$\frac{t}{q} = \frac{1}{k_2 q_e^2} + \frac{t}{q_e} \tag{7}$$

where k_2 is the pseudo-second-order rate constant ($mg\,g^{-1}\,min^{-1}$), q_e and q represent the amount of Sn (II) adsorbed ($mg\,g^{-1}$) at equilibrium and at any time.

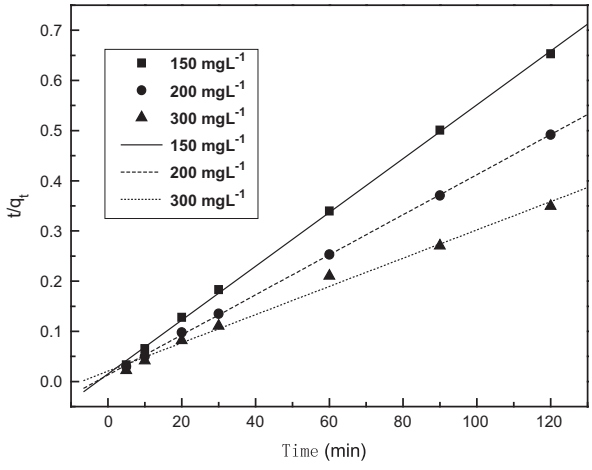

Fig. 13. Pseudo-second order kinetic plots for the removal of Sn(II) by EG at room temperature.

Table 2
Kinetic parameters for pseudo-first-order adsorption rate expressions

Concentration ($mg\,L^{-1}$)	Parameters of pseudo-first-order		
	q_e ($mg\,g^{-1}$)	k_1 (min^{-1})	R^2
150	40.08	0.0262	0.9830
200	89.29	0.0467	0.9875
300	154.60	0.0257	0.8750

Table 3
Kinetic parameters for pseudo-second-order adsorption rate expressions

Concentration ($mg\,L^{-1}$)	Parameters of pseudo-second-order			
	k_2 ($g\,mg^{-1}\,min^{-1}$)	h ($mg\,g^{-1}\,min^{-1}$)	R^2	q_e ($mg\,g^{-1}$)
150	0.0019	66.23	0.9994	186.6
200	0.0012	77.40	0.9997	250.6
300	0.0004	48.76	0.9913	354.6

The equilibrium adsorption capacity (q_e), and the pseudo-second-order constants (k_2) can be determined experimentally from the slope and intercept of plot $\frac{t}{q}$ vs. t (Fig. 13).

All kinetic parameters and correlation coefficients are listed in Tables 2 and 3. It can be seen from Fig. 11 and Table 2 that the pseudo-first-order kinetic curves do not give a good fit to the experimental kinetic data. As a result, it was suggested that the adsorption of Sn(II) onto EG did not follow the pseudo-first-order model. On the contrary, the results presented an ideal fit to the pseudo-second-order model with extremely high R^2 (0.9913–0.9997).

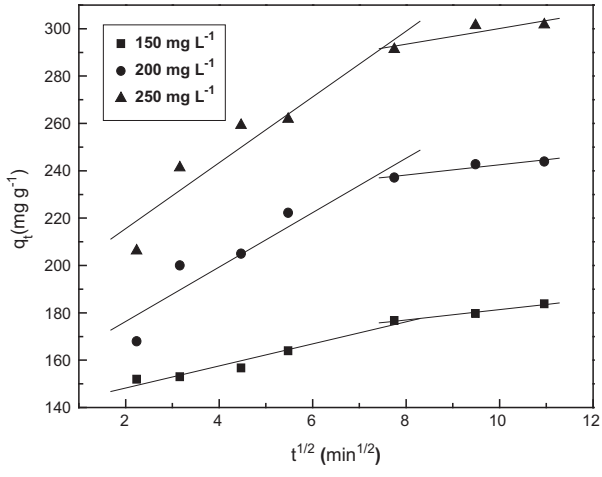

Fig. 14. Intraparticle diffusion plot for the adsorption of Sn (II) onto EG.

Table 4
Intraparticle diffusion rate parameter at different initial concentration

Initial concentration (mg L^{-1})	K_{p1} (mg g^{-1} $min^{-1/2}$)	K_{p2} (mg g^{-1} $min^{-1/2}$)	R_1^2	R_2^2	C_1	C_2
150	4.66	2.188	0.9531	0.9826	139.0	159.5
200	11.49	2.155	0.8925	0.9034	153.4	221.0
250	13.91	3.305	0.9080	0.8104	187.8	267.1

3.5. Adsorption mechanism

To gain insight into the mechanisms and rate-controlling steps affecting the kinetics of adsorption, the intraparticle diffusion model is shown as:

$$q_t = k_{pi} t^{1/2} + C_i \quad (8)$$

where k_{pi} (mg g^{-1} $min^{1/2}$) is the intraparticle diffusion rate constant of stage i, and C_i is the intercept of stage i. Values of C provide information on the thickness of the boundary layer—the larger the intercept, the greater the boundary layer effect. To follow the intraparticle diffusion model, a plot of q_t compared with $t^{1/2}$ should give a linear line, where a slope represents k_p, and the intercept represents C.

Fig. 14 shows that the amount of Sn(II) adsorbed compared with $t^{1/2}$ for the intraparticle transport of Sn(II) by EG at different initial concentrations. The plots displayed multilinearity, indicating two steps that occurred in the process. The first, sharper portion was the external surface adsorption or the instantaneous adsorption. The second portion was the gradual adsorption stage where intraparticle diffusion was rate-limiting [17].

Table 4 lists the corresponding model parameters based on the equation above. For all initial concentrations, k_{p1} was higher than k_{p2}, and C_2 was larger than C_1. This indicated that the rate of metal removal was higher in the beginning due to larger surface areas of the adsorbent available for adsorption of metal ions. After the adsorbed material formed a thick layer (caused by the inter-ionic attraction and molecular association), the capacity of adsorbent was exhausted and the uptake rate was controlled by the rate at which the adsorbate was transported from the exterior to the interior sites of the adsorbent particles. None of the plots passed through the origin (Fig. 14), which revealed that the intraparticle diffusion was part of the adsorption process but was not the only rate-controlling step. Some other mechanisms such as complexes or ion-exchange may also control the rate of adsorption [18].

4. Conclusions

The present study demonstrates that the EG is an effective and novel adsorbent for the removal of Sn(II) in aqueous solutions. The adsorption is highly dependent on pH, adsorbent dosage, initial concentration, and temperature. The equilibrium data are identical with Langmuir and the isotherm model, and the maximum adsorption capacity of Sn(II) on EG is 378.78 mg g^{-1}.

Acknowledgments

The authors gratefully acknowledge Innovation Program of Shanghai Municipal Education Commission (12zz069), Shanghai Municipal Natural Science Foundation (11ZR1400400), and Fundamental Research Funds for the Central Universities (12D11303).

References

[1] K.G. Sreejalekshmi, K. Anoop Krishnan, T.S. Anirudhan, Adsorption of Pb(II) and Pb(II)-citric acid on sawdust activated carbon: Kinetic and equilibrium isotherm studies, J. Hazard. Mater. 161 (2009) 1506–1513.
[2] M. Kobya, E. Demirbas, E. Senturk, M. Ince, Adsorption of heavy metal ions from aqueous solutions by activated carbon prepared from apricot stone, Bioresour. Technol. 96 (2005) 1518–1521.
[3] J. Zhang, L. Wang, S. Chen, Adsorption of tin cations in water by treated rubbish remains, JBUU (Natural Sciences). 20 (2006) 76–79.
[4] S. Cheng, Study on the adsorption of surfactant and Tin(II) ion by activated carbon at high acidity, Chem. Res. Appl. 16 (2004) 109–110.
[5] M. Zhao, P. Liu, Adsorption of methylene blue from aqueous solution by modified expanded graphite power, Desalination 249 (2009) 331–336.
[6] A.D. Lucking, L. Pan, D.L. Narayanan, C.E.B. Clifford, Effect of expanded graphite lattice in exfoliated graphite nanofibers on hydrogen storage, J. Phys. Chem. B. 109 (2005) 12710–12717.
[7] A. Bhattacharya, A. Hazra, S. Chatterjee, P. Sen, S. Laha, I. Basumallick, Expanded graphite as an electrode material for an alcohol fuel cell, J. Power Sources. 136 (2004) 208–210.
[8] C. Calas-Blanchard, T. Noguer, M. Comtat, S. Mauran, J.L. Marty, Potentialities of expanded natural graphite as a new transducer for NAD^+-dependent dehydrogenase amperometric biosensors, Anal. Chim. Acta. 484 (2003) 25–31.
[9] W. Li, C. Han, W. Liu, M.H. Zhang, K.Y. Tao, Expanded graphite applied in the catalytic process as a catalyst support, Catal. Today 125 (2007) 278–281.

[10] W.C. Shen, S.Z. Wen, N.Z. Cao, L. Zheng, W. Zhou, Y.J. Liu, J.L. Gu, Expanded graphite—A new kind of biomedical material, Carbon 37 (1999) 356–358.
[11] L.R. Radovic, Chemistry and Physics of Carbon, Taylor & Francis, New York, NY, 2008.
[12] O.S. Josyulu, J. Sobhnadari, The far-infrared spectra of some mixed cobalt zinc and magnesium zinc ferrites, Phys. Status Solidi (A) 65 (1981) 479–483.
[13] M. Eibshutz, G. Gorodetsky, S. Shtrikman, D. Treves, Differential thermal analysis and mossbauer studies in rare-earth orthofer-rites, J. Appl. Phys. 35 (1964) 1071.
[14] S.Z. Mohammadi, M.A. Karimi, D. Afzali, F. Mansouri, Removal of Pb(II) from aqueous solutions using activated carbon from Sea-buckthorn Stones by chemical activation, Desalination 262 (2010) 86–93.
[15] P. Das Saha, S. Chowdhury, S. Datta, S.K. Sanyal, Removal of Pb(II) from aqueous solutions by adsorption onto clayey soil of Indian origin: Equilibrium, kinetic and thermodynamic profile, Korean J. Chem. Eng. 29 (2012) 1086–1093.
[16] A. Sharma, K.G. Bhattacharyya, Adsorption of chromium(VI) on *Azadirachta indica* (Neem) leaf powder, Adsorption 10 (2004) 327–338.
[17] F.C. Wu, R.L. Tseng, R.S. Juang, Comparisons of porous and adsorption properties of carbons activated by steam and KOH, J. Colloid Interface Sci. 283 (2005) 49–56.
[18] W.H. Cheung, Y.S. Szeto, G. McKay, Intraparticle diffusion processes during acid dye adsorption onto chitosan, Bioresour. Technol. 98 (2007) 2897–2904.